Journal of Clinical and Translational Hepatology **2026**
DOI: 10.14218/JCTH.2026.00356

Original Article

High Frequency of Circulating IL-4R$^+$SELL$^+$ Naïve B Cells Is Associated with Functional Cure in Chronic Hepatitis B Patients Receiving Antiviral Treatment

Lili Tang[1,2], Chunmei Bao[3], Cheng Zhen[2], Huan Wang[2], Chao Zhang[2], Yang Zhang[2], Honghong Liu[4], Jinwen Song[2], Yanmei Jiao[2], Tao Yang[2], Yue Yuan[2], Jinhong Yuan[2], Yingying Gao[2], Yangliu Chen[2], Lin Cao[2], Jing Li[2], Jun-Liang Fu[1,2], Fu-Sheng Wang[1,2*] and Ruonan Xu[2*]

[1]Peking University 302 Clinical Medical School, Beijing, China; [2]Senior Department of Infectious Diseases, Chinese PLA General Hospital, National Clinical Research Center for Infectious Diseases, Beijing, China; [3]Department of Clinical Laboratory, The Fifth Medical Center of Chinese PLA General Hospital, Beijing, China; [4]Out-patient Department of Day Diagnosis and Treatment, The Fifth Medical Center of Chinese PLA General Hospital, Beijing, China

Received: May 06, 2026 | **Revised:** July 07, 2026 | **Accepted:** July 29, 2026 | **Published online:** August 26, 2026

Abstract

Background and Aims: Although hepatitis B surface antigen (HBsAg)-specific B cells have been partially characterized in chronic hepatitis B (CHB), the role of Naïve B cells and their potential relevance to functional cure remain insufficiently explored. Here, we aimed to characterize the naïve B-cell subsets between cured and uncured patients with CHB. ***Methods:*** In this retrospective study, we applied single-cell RNA sequencing to compare peripheral B-cell profiles between cured and uncured CHB patients. Key findings were validated by flow cytometry in an independent cohort and further supported in a nucleos(t)ide analog monotherapy cohort stratified by HBsAg levels. ***Results:*** Single-cell RNA sequencing characterized two Naïve B-cell subsets, designated IL-4R$^+$SELL$^+$ and IL-4R$^-$SELL$^-$ Naïve B cells, which were differentially distributed between functionally cured and uncured patients. Cured patients showed higher frequencies of total B cells and IL-4R$^+$SELL$^+$ Naïve B cells than uncured patients. In contrast, uncured patients exhibited persistent hyperactivation of type I interferon signaling in both Naïve and memory B cells. The IL-4R$^+$SELL$^+$ subset showed a transcriptional signature associated with germinal center biology and exhibited stronger ligand–receptor interactions with CD40LG$^+$CD4$^+$ T cells. Notably, the frequency of the IL-4R$^+$SELL$^+$ subset was inversely correlated with HBsAg levels. Consistently, patients with lower HBsAg levels also exhibited significantly higher frequencies of IL-4R$^+$SELL$^+$ Naïve B cells compared with those with high HBsAg levels. ***Conclusions:*** Collectively, these findings indicate that the IL-4R$^+$SELL$^+$ Naïve B-cell subset is characterized by germinal center-related responses and enhanced T-cell-mediated help and may serve as an immunological component associated with functional cure in CHB.

Citation of this article: Tang L, Bao C, Zhen C, Wang H, Zhang C, Zhang Y, *et al*. High Frequency of Circulating IL-4R$^+$SELL$^+$ Naïve B Cells Is Associated with Functional Cure in Chronic Hepatitis B Patients Receiving Antiviral Treatment. J Clin Transl Hepatol 2026. doi: 10.14218/JCTH.2026.00356.

Introduction

The World Health Organization estimates that 257 million people worldwide are chronically infected with hepatitis B virus (HBV).[1] The generation of neutralizing antibodies against hepatitis B surface antigen (HBsAg) represents a critical immunological event associated with HBsAg loss and is considered essential for achieving a functional cure of chronic hepatitis B (CHB).[2,3] Clinical observations that B-cell-depleting therapies, such as rituximab, can induce severe HBV reactivation even in individuals with resolved infection further highlight the critical role of B cells in maintaining long-term HBV immune control in CHB.[4–7]

Previous studies have reported that patients with CHB have hyperactivated circulating B cells characterized by increased expression of activation-related genes, including CD83, CD300c, CXCR4, and CD69.[8,9] The coexistence of this systemic B-cell activation with an expanded population of atypical memory B cells suggests that chronic antigenic stimulation may drive phenotypic and functional exhaustion in CHB.[10–13] Recent advances, particularly single-cell RNA sequencing (scRNA-seq), have revealed significant heterogeneity in circulating B cells, providing new insights into their transcriptional and functional diversity.[14,15] In CHB, most studies have primarily focused on HBsAg-specific or memory B-cell compartments,[11–13,16,17] whereas Naïve B cells, despite being the most abundant subset in circulation, remain insufficiently studied.

Keywords: Chronic hepatitis B; Hepatitis B surface antigen; HBsAg; Naïve B cells; B cells; Functional cure; Single-cell RNA sequencing.

***Correspondence to:** Ruonan Xu, Senior Department of Infectious Diseases, Chinese PLA General Hospital, National Clinical Research Center for Infectious Diseases, 100 Western 4th Ring Middle Road, Beijing 100039, China. Tel: +86-10-66933241, E-mail: xuruonan2004@aliyun.com; Fu-Sheng Wang, Senior Department of Infectious Diseases, Chinese PLA General Hospital, National Clinical Research Center for Infectious Diseases; Peking University 302 Clinical Medical School, 100 Western 4th Ring Middle Road, Beijing 100039, China. ORCID: https://orcid.org/0000-0002-8043-6685. Tel: +86-10-66933241, E-mail: fswang302@163.com.

Naïve B cells maintain considerable developmental plasticity and can give rise to new antigen-specific clones through germinal center reactions. During chronic viral infections, persistent antigen exposure may impair pre-existing memory B cells or limit antibody affinity maturation.[18] Under such conditions, Naïve B cells can serve as a reservoir for replenishing the humoral repertoire and potentially contribute to renewed antiviral immunity.[19] These observations raise the possibility that Naïve B-cell biology may play an underrecognized role in immune control of CHB.

Here, we performed integrated scRNA-seq and flow cytometry analyses of B cells from nucleos(t)ide analog (NA)-treated CHB patients who received add-on pegylated interferon alpha (PEG-IFNα) therapy and achieved either HBsAg loss or persistent HBsAg positivity. This approach allowed us to comprehensively compare Naïve B-cell heterogeneity between cured and uncured patients. We identified two transcriptionally distinct Naïve B-cell subsets, designated IL-4R$^+$SELL$^+$ and IL-4R$^-$SELL$^-$ Naïve B cells. The IL-4R$^+$SELL$^+$ Naïve B-cell subset was present at higher frequencies in patients achieving functional cure and was associated with germinal center-related transcriptional features and enhanced help from CD40LG$^+$CD4$^+$ T cells. Notably, the frequency of the IL-4R$^+$SELL$^+$ Naïve B-cell subset was inversely correlated with on-treatment HBsAg levels but independent of patient age. These findings highlight previously unrecognized Naïve B-cell heterogeneity and suggest that specific Naïve B-cell states may be linked to immune control and HBsAg loss in CHB.

Methods

Study design and population

This was a retrospective study with three independent cohorts. Both Cohort 1 and Cohort 2 received PEG-IFNα add-on therapy following NA treatment. Cohort 1 included 11 patients with CHB (6 functionally cured and 5 uncured), whose peripheral blood mononuclear cells (PBMCs) were used for scRNA-seq analysis. Cohort 2 comprised 12 cured and 16 uncured patients and was used to validate the findings from Cohort 1 by flow cytometry. Inclusion criteria for patients receiving PEG-IFNα add-on therapy were as follows: (1) confirmed CHB diagnosis according to the Guideline of Prevention and Treatment for Chronic Hepatitis B, with HBsAg positivity for at least 6 months; (2) age 18–65 years at enrollment; (3) continuous NA treatment for at least 12 months prior to PEG-IFNα initiation; and (4) at baseline before PEG-IFNα add-on therapy, HBsAg levels < 1,500 IU/mL, hepatitis B e antigen (HBeAg) seroconversion, and HBV DNA < 10 IU/mL. Exclusion criteria were as follows: (1) human immunodeficiency virus (HIV) co-infection; (2) decompensated cirrhosis; (3) hepatic failure; (4) hepatocellular carcinoma; (5) history of solid organ transplantation; (6) active autoimmune disorders; (7) severe cardiovascular, cerebrovascular, renal, or neurological comorbidities; and (8) current or planned pregnancy.

Functional cure was defined as sustained HBsAg loss (<0.05 IU/mL) after treatment discontinuation, with or without hepatitis B surface antibody seroconversion, undetectable serum HBV DNA, and normalization of liver enzymes (alanine aminotransferase [ALT] and aspartate aminotransferase [AST]). Based on this definition, patients were classified as cured or uncured according to their outcomes at week 96 after treatment initiation. For cured patients, samples were collected at the visit when HBsAg loss was first documented. For the uncured group, samples were obtained at cross-sectional visits during PEG-IFNα therapy, including patients who had not achieved serological clearance by the end of observation (96 weeks). After week-96 outcomes had been confirmed, samples were retrospectively selected from archived specimens, and patients were classified as cured or uncured accordingly. The two groups were matched at enrollment for age, sex, baseline HBsAg levels, and PEG-IFNα treatment duration (Supplementary Fig. 1).

To evaluate the association between B-cell subset frequencies and HBsAg levels independently of interferon therapy, Cohort 3 was enrolled and included 17 patients with CHB. These patients received NA therapy for at least 2 years and maintained sustained virological suppression (HBV DNA < 10 IU/mL on at least 3 consecutive tests over 6 months). Samples were collected at a single cross-sectional visit, and patients were retrospectively stratified into low HBsAg (<100 IU/mL, n = 8) and high HBsAg (>1,000 IU/mL, n = 9) groups based on their HBsAg levels at sampling (Supplementary Table 1).

PBMC isolation and processing

Peripheral blood samples were collected in lithium-heparin vacutainer tubes (BD Biosciences, Franklin Lakes, NJ). PBMCs and plasma were isolated by density gradient centrifugation (400 × g, 20 °C for 20 min) using Ficoll-Paque PLUS (TBD Science, Tianjin). Following two washes with phosphate-buffered saline (PBS, Gibco), PBMCs were resuspended in medium consisting of 90% heat-inactivated fetal bovine serum (FBS, Gibco, A5669701) and 10% dimethyl sulfoxide (DMSO, Sigma-Aldrich, St. Louis, MO). Cells were aliquoted at 5 × 10^6 cells/mL in cryovials and transferred to a controlled-rate freezing container for gradual cooling before long-term storage in liquid nitrogen.

scRNA-seq data filtering, quality control, and integration

Eleven patients were used for scRNA-seq, including 6 cured and 5 uncured cases. The isolated cells were sequenced using the 10x Chromium single-cell platform (10x Genomics, USA, CG000527) according to the manufacturer's instructions. scRNA-seq data filtering and quality control were performed using CellRanger against the GRCh38 human reference. Genes detected in fewer than 3 cells were removed. High-quality cells were retained based on the following criteria: expressed genes between 200 and 5,000, mitochondrial transcript ratio < 10%, and unique molecular identifier counts between 500 and 25,000. Potential doublets were identified and removed using DoubletFinder. We then applied Seurat (5.1.0) to perform data scaling, transformation, clustering, dimensionality reduction, differential expression analyses, and most visualization procedures.

Differential gene expression, pathway enrichment, and Human Protein Atlas (HPA) analysis

Differentially expressed genes (DEGs) were identified using the FindMarkers function in the Seurat package with the Wilcoxon rank-sum test. *P*-values were adjusted for multiple testing using the Benjamini–Hochberg method. Genes with an adjusted *P*-value < 0.05 and |log2 fold change| > 0.5 were considered significantly differentially expressed. Gene set enrichment analysis was performed using the clusterProfiler package. Significantly upregulated genes were compared with germinal center B-cell signature genes from the HPA to identify overlapping germinal center-associated genes.

Calculation of functional module scores at the single-cell level

To quantify pathway activity in B-cell subsets, we performed gene signature scoring using AUCell (v1.24.0). Gene sets

were curated from MSigDB (v7.5.1) via the msigdbr package (v7.5.1), focusing on GO terms (C5), including GOBP_RESPONSE_TO_TYPE_I_INTERFERON, GOBP_B_CELL_ACTIVATION, GOBP_OXIDATIVE_PHOSPHORYLATION, and GOBP_ATP_SYNTHESIS_COUPLED_ELECTRON_TRANSPORT. Scores were calculated from log1p-transformed normalized counts, with AUC thresholds automatically determined via distribution knee points (minimum threshold: 5% of the maximum theoretical AUC). Cells with <200 detected genes were excluded. Differential activity across subsets was assessed using Wilcoxon rank-sum tests with Benjamini–Hochberg correction (false discovery rate [FDR] < 0.05).

Single-cell trajectory analysis

To infer the differentiation relationship among B-cell subtypes, pseudotime analysis was performed using Monocle2 (v2.30.0). Highly variable genes identified during single-cell clustering analysis were used to construct the trajectory. Dimensionality reduction was performed using the DDRTree algorithm implemented in the reduceDimension function. The trajectory was rooted at the predominant IGHD$^+$ B-cell population, representing Naïve B cells and the earliest stage of B-cell differentiation. Branch points along the trajectory were identified to represent potential cell fate decisions during B-cell differentiation. Cell states along the pseudotime trajectory were visualized using the plot_cell_trajectory function.

Prediction of cell –cell communications using CellChat

Cell–cell communication analysis was performed using CellChat (v2.1.2). The normalized gene expression matrix and annotated major cell types were used as input, with a specific focus on interactions between T- and B-cell subsets. The CellChatDB.human database was used as the reference ligand–receptor interaction dataset. Overexpressed genes and overexpressed ligand–receptor interactions were identified using the identifyOverExpressedGenes and identifyOverExpressedInteractions functions, respectively. Cell–cell communication probabilities were computed using the computeCommunProb function, and interactions supported by fewer than five cells in any involved cell type were filtered out to ensure robustness. Differential interaction strength and inferred signaling networks were compared by aggregating all ligand–receptor pairs using the netVisual_circle and netVisual_aggregate functions.

Flow cytometry analysis

The cohort 2 (12 cured and 16 uncured) was used for flow cytometry analysis. Paired specimens from an early time point (before HBsAg loss) and at HBsAg loss were available for 7 of the 12 cured patients. For the uncured group, paired specimens from corresponding early time points were available for 3 of the 16 patients (designated as Uncured_T1 in figures).

Cryopreserved PBMCs were thawed at 37 °C and stained for surface and intracellular markers using optimized protocols. Briefly, cells were resuspended in fluorescence-activated cell sorting (FACS) buffer (2% FBS/PBS) and incubated with pre-titrated surface antibody cocktails (Supplementary Table 2) for 30 min at 4 °C. After washing twice with cold FACS buffer (300 × g, 5 min), cells were fixed and permeabilized using the BD Cytofix/Cytoperm™ Kit for 30 min at room temperature. Following permeabilization, cells were incubated with Fc receptor block (5 μL/test) for 15 min at 4 °C, then stained with recombinant MX-1 protein (kindly provided by Prof. Liguo Zhang, Institute of Biophysics, Chinese Academy of Sciences) for 30 min at 4 °C. After washing with Perm/Wash buffer, cells were stained with an anti-mouse immunoglobulin G (igG) fluorescein isothiocyanate (FITC)-conjugated secondary antibody for 30 min at 4 °C. Cells were then washed with FACS buffer and resuspended in 200 μL of FACS buffer. Samples were acquired on a BD FACSAria™ III, and data were analyzed using FlowJo v10.8.1.

Statistical analyses

Statistical analyses were conducted using GraphPad Prism (version 8.0) and R software (version 4.3.2). Continuous variables are presented as median (interquartile range [IQR]). Differences between two independent groups were analyzed using the Mann–Whitney U test, and paired comparisons were performed using the Wilcoxon signed-rank test. Spearman's rank correlation coefficient was used to evaluate correlations between quantitative variables. Categorical variables were expressed as numbers (percentages) and compared using the chi-square test. A two-sided *P*-value < 0.05 was considered statistically significant.

Results

High frequency of peripheral IL-4R$^+$SELL$^+$ Naïve B cells in cured patients receiving antiviral treatment

We performed scRNA-seq on PBMCs isolated from 11 NA-treated HBeAg-negative CHB patients with or without functional cure following sequential PEG-IFNα add-on therapy, 6 of whom achieved functional cure and 5 of whom did not (Fig. 1A). Their clinical information is detailed in Table 1. After rigorous quality control, cell populations were identified through unsupervised clustering, with clusters expressing canonical lineage markers retained for analysis (Fig. 1B and C). The proportions of cell populations within PBMCs were calculated (Fig. 1D). Of these, only B cells displayed a significant intergroup difference, showing a higher frequency in the cured group compared with the uncured group (P = 0.044) (Fig. 1E). In contrast, the other lymphocyte subsets (NK cells, CD4$^+$ T cells, CD8$^+$ T cells, monocytes, and dendritic cells) showed no significant differences between the two groups (Supplementary Fig. 2A). This suggests a potential association between B-cell reconstitution and functional cure during PEG-IFNα-based therapy. B cells were then extracted for further analysis. Unsupervised clustering revealed two Naïve B-cell subsets and three memory B-cell subsets (Fig. 1F and G), annotated according to previously reported marker genes.[20,21] The two Naïve subsets were distinguished by differential expression of *NR4A1, CD72,* and *PLD4* versus *FCER2, IL4R, SELL,* and *PLPP5.* Pre-memory B cells were identified by elevated *TNFRSF13B* and *GPR183* expression with low levels of IGHD and IGHM. Atypical memory B cells were identified by high expression of *FCRL5, FCRL3*, and *SOX5,* whereas classical memory B cells were identified by high expression of *SELL, COCH, CD80,* and *CD86*.

Naïve B cells accounted for more than 50% of the total peripheral B-cell population in our cohort (Fig. 1H). We compared all B-cell subsets and found that the cured group had a significantly higher frequency of IL-4R$^+$SELL$^+$ Naïve B cells compared with the uncured group (P = 0.033), while no significant intergroup differences were observed for the other subsets (Fig. 1I, Supplementary Fig. 2B). Together, these findings suggest that IL-4R$^+$SELL$^+$ Naïve B cells may be associated with favorable treatment outcomes following PEG-IFNα therapy.

IL-4R$^+$SELL$^+$ Naïve B cells exhibit distinct transcriptional and phenotypic features

We first compared the differential expression of genes be-

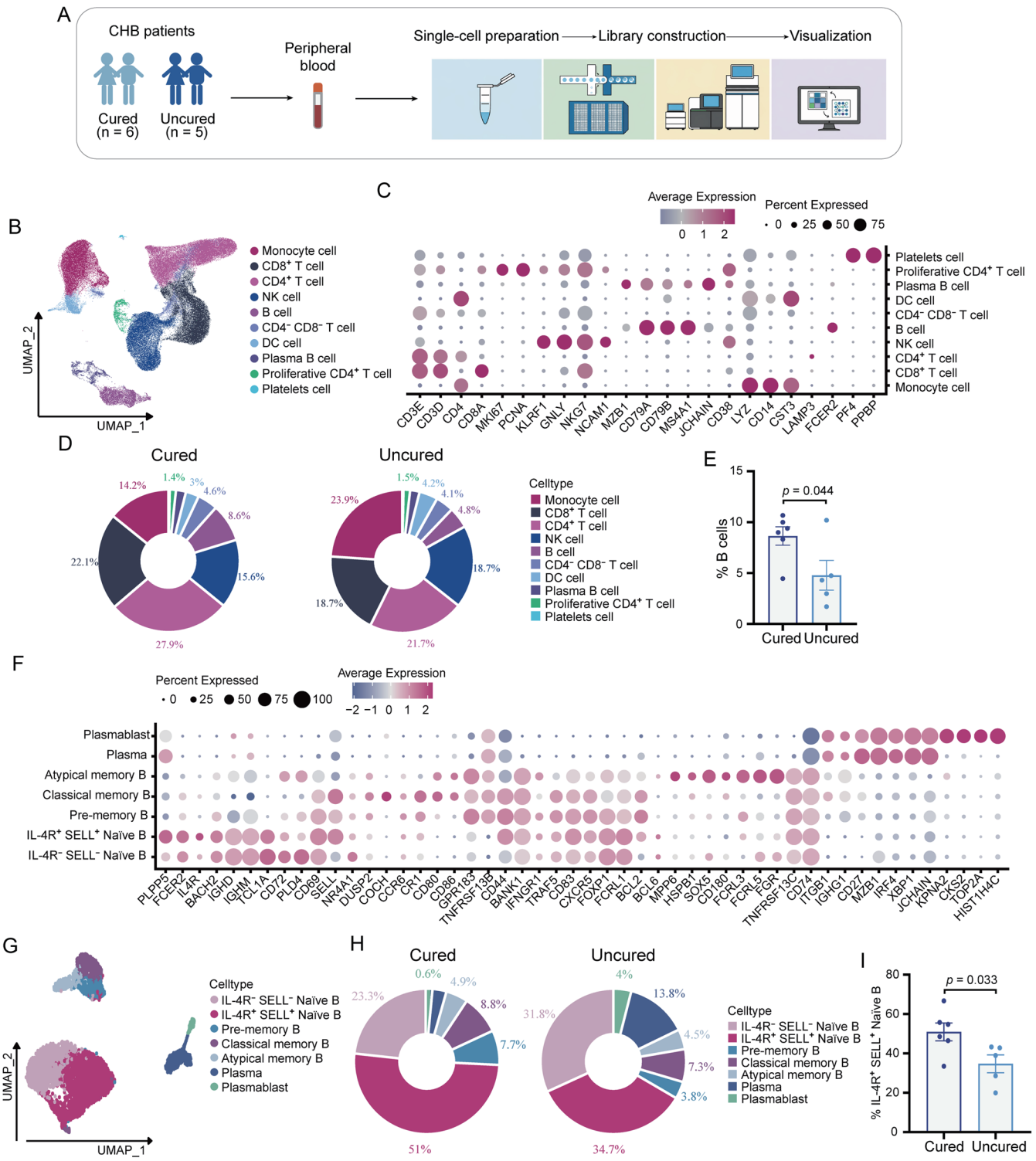

Fig. 1. High frequency of peripheral IL-4R^{+}SELL^{+} Naïve B cells in cured patients receiving antiviral treatment. (A) Flowchart of the experiment. (B) UMAP visualization of 104,341 PBMCs clustered into 10 distinct cell subpopulations. (C) Dot plot displaying cluster-defining marker gene expression. Color intensity indicates maximum scaled mean expression, and dot size represents the percentage of cells expressing these genes. (D) Distribution of PBMC subsets in cured and uncured groups. (E) Comparison of B-cell frequencies between cured and uncured patient groups. (F) Canonical markers distinguishing major B-cell subsets. Color intensity indicates maximum scaled mean expression, while dot size represents the percentage of cells expressing each gene. (G) A total of 7,080 B cells were isolated and subsequently clustered using UMAP visualization. (H) Distribution of B-cell subsets in cured and uncured groups. (I) Differential analysis of IL-4R^{+}SELL^{+} Naïve B-cell frequencies between the two groups. Data are presented as mean ± SEM, and differences were analyzed with the Mann–Whitney U test. Statistical significance was set at $P < 0.05$. CHB, Chronic hepatitis B; SEM, standard error of the mean; PBMC, peripheral blood mononuclear cell; UMAP, Uniform Manifold Approximation and Projection.

Table 1. Characteristics of the patients for single-cell RNA sequencing

	Cured (n = 6)	Uncured (n = 5)	*P-value*
Age (Years)	40 (36–47)	42 (39–46)	0.65
Male, n (%)	5 (83.3)	4 (80)	>0.99
Baseline HBsAg (IU/mL)[#]	138.4 (28.9–943.5)	419.9 (297.8–1,045.0)	0.55
Baseline HBeAg seroconversion, n (%)[#]	6 (100)	5 (100)	>0.99
Baseline HBV DNA clearance, n (%)[#]	6 (100)	5 (100)	0.99
Baseline ALT (U/L)[#]	31.0 (17.8–71.0)	45.0 (28.5–51.0)	0.31
HBsAg at sampling (IU/mL)[*]	0.05	147.5 (8.6–291.2)	<0.01
ALT at sampling (U/L)[*]	58.0 (27.8–179.0)	45.0 (37.5–45.5)	0.82
PEG-IFNα treatment and follow-up duration at the time of blood sampling (weeks)	55 (30–77)[†]	96[※]	-

Median (IQR). [#]Represents the HBsAg level, HBeAg, HBV DNA, and ALT at the time of PEG-IFNα administration. *Represents the HBsAg level and ALT at the time of sample collection. [†]Blood samples from the cured group were collected when HBsAg loss was first documented, with or without hepatitis B surface antibody seroconversion. [※]Patients in the uncured group received standard treatment and were followed up for 96 weeks without achieving HBsAg clearance. HBV, hepatitis B virus; HBsAg, Hepatitis B surface antigen; HBeAg, Hepatitis B e antigen; IQR, interquartile range; ALT, Alanine aminotransferase; AST, Aspartate aminotransferase; PEG-IFNα, Pegylated interferon-alpha.

tween IL-4R$^-$SELL$^-$ Naïve B cells and IL-4R$^+$SELL$^+$ Naïve B cells. IL-4R$^+$SELL$^+$ Naïve B cells exhibited high expression of *IL4R, BACH2, FOXO1, FCRL1, CXCR4, CD83*, and *CD69*. IL-4R$^-$SELL$^-$ Naïve B cells exhibited high expression of *FCRL5, PLD4, CD38, CD72, MZB1, STAT6, IRF4, NR4A1*, and *JUNB* (Fig. 2A). We further examined the expression of functional gene categories, including activation markers (*CD69* and *CD83*), migration receptors (*CCR7* and *CXCR5*), interferon-stimulated genes (*ISG15* and *MX1*), anti-apoptotic factors (*BCL2*), and immunoregulatory molecules (*LGALS9*), revealing differences in activation and chemotaxis between the two Naïve B-cell subsets (Fig. 2B). Consistently, pathway enrichment analysis demonstrated that the antigen receptor-mediated signaling pathway and B-cell receptor signaling pathway were enhanced in IL-4R$^+$SELL$^+$ Naïve B cells, whereas the response to type I interferon, positive regulation of Erbb signaling pathway, and G protein-coupled receptor signaling pathway were activated in IL-4R$^-$SELL$^-$ Naïve B cells (Fig. 2C).

We next compared transcriptional profiles between cured and uncured patients within each Naïve B-cell subset. In the IL-4R$^+$SELL$^+$ subset, cured patients showed enrichment of oxidative phosphorylation and adenosine triphosphate (ATP) metabolic pathways, whereas uncured patients exhibited increased immune activation-related signatures and protein kinase activity (Fig. 2D). A similar pattern was observed in the IL-4R$^-$SELL$^-$ subset: cured patients exhibited increased oxidative phosphorylation, whereas uncured patients showed preferential enrichment of long-chain fatty acid metabolism and NF-κB-inducing kinase activity (Fig. 2E). Finally, to assess whether IL-4R$^+$SELL$^+$ Naïve B cells exhibit transcriptional features associated with germinal center competence, the top 25 genes upregulated in IL-4R$^+$SELL$^+$ Naïve B cells relative to IL-4R$^-$SELL$^-$ Naïve B cells were compared with germinal center B-cell signature genes from the HPA to identify overlapping germinal center-associated genes (Fig. 2F), suggesting that IL-4R$^+$SELL$^+$ Naïve B cells may be primed for germinal center participation.

Divergent trajectories of IL-4R$^+$SELL$^+$ Naïve B cells and T-cell help in cured versus uncured patients

We next profiled the memory B-cell compartment. Each subset exhibited clear group-specific differences in differential gene expression and pathway enrichment (Fig. 3A–C). Memory B cells from uncured patients consistently showed enrichment of type I interferon response and B-cell activation pathways, whereas those from cured patients exhibited increased activity of oxidative phosphorylation and ATP synthesis-coupled electron transport. To determine whether these transcriptional patterns were limited to memory B cells or reflected a broader shift across the B-cell lineage, we assessed pathway activity across all Naïve and memory B-cell subsets using AUCell. The same dichotomy was observed across the entire B-cell compartment, with uncured patients showing elevated interferon-response signatures and cured patients exhibiting stronger oxidative phosphorylation activity (Fig. 3D).

To further explore lineage relationships among B-cell subsets, we performed trajectory and correlation analyses. Notably, in uncured patients, IL-4R$^-$SELL$^-$ Naïve B cells exhibited a transcriptional trajectory toward the atypical memory lineage (Fig. 4A). Consistently, IL-4R$^-$SELL$^-$ Naïve B cells negatively correlated with pre-memory B cells, whereas pre-memory B cells positively correlated with classical memory B cells (Fig. 4B). Given the different Naïve B-cell states, we next investigated whether T-cell help might contribute to the differential outcomes between cured and uncured patients. T cells were extracted from the scRNA-seq data and clustered as previously described (Supplementary Fig. 3A and B). Analysis showed that in cured patients, CD40L$^+$CD4$^+$ T cells and CCR7$^+$CD4$^+$ T cells exhibited a biased helper preference toward IL-4R$^+$SELL$^+$ Naïve B cells, whereas this bias was absent in uncured patients (Fig. 4C). To further understand the basis of this differential helper pattern, we examined the major signaling pathways contributing to T–B cell communication. The analysis revealed the macrophage migration inhibitory factor signaling pathway as the dominant contributor, consistent with the enhanced T-cell helper engagement observed in cured patients (Fig. 4D).

High frequency of IL-4R$^+$SELL$^+$ Naïve B cells was further confirmed in cured patients with CHB

To confirm the reproducibility of the B-cell subset differences, we performed flow cytometry analysis in an independent cohort of CHB patients undergoing sequential PEG-IFNα add-on therapy following NAs treatment (cohort 2; Supplementary Fig. 1). Demographic, clinical, and laboratory characteristics are detailed in Supplementary Ta-

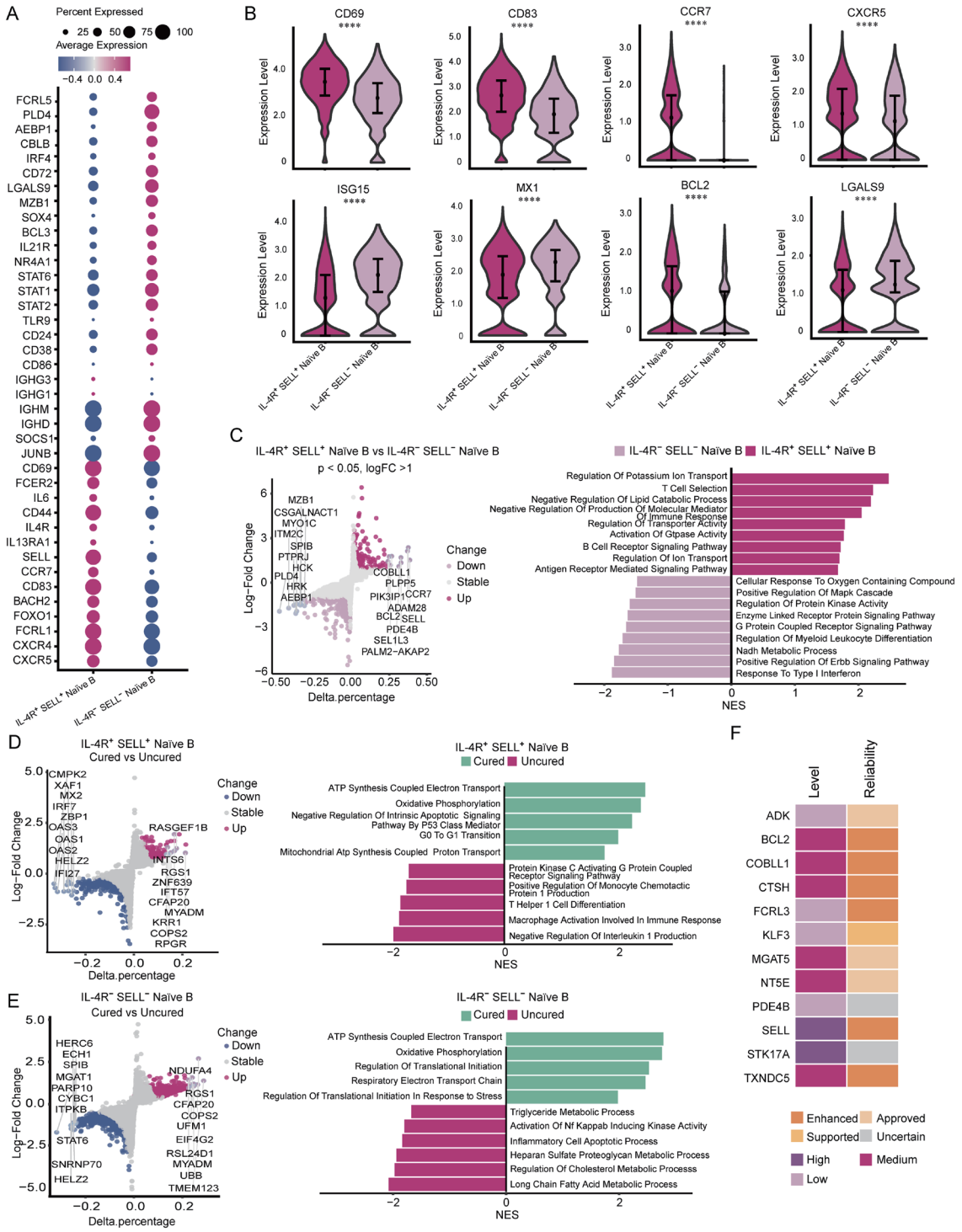

Fig. 2. IL-4R^{+}SELL^{+} Naïve B cells exhibit distinct transcriptional and phenotypic features. (A) Dot plot showing differential marker gene expression between IL-4R^{+}SELL^{+} and IL-4R^{-}SELL^{-} Naïve B cells. (B) Comparative analysis of gene expression profiles between IL-4R^{+}SELL^{+} Naïve B cells and IL-4R^{-}SELL^{-} Naïve B cells. (C) Volcano plot of DESeq2 analysis comparing gene expression profiles between IL-4R^{+}SELL^{+} and IL-4R^{-}SELL^{-} Naïve B cells (left panel), and representative GSEA of differentially expressed genes between the two clusters (right panel). (D–E) Volcano plots showing DEGs from DESeq2 analysis comparing IL-4R^{+}SELL^{+} Naïve B cells and IL-4R^{-}SELL^{-} Naïve B cells between cured and uncured groups (left panel), and GSEA analysis of DEGs between cured and uncured groups for each Naïve cluster (right panel). (F) The top 25 upregulated genes in IL-4R^{+}SELL^{+} Naïve B cells versus IL-4R^{-}SELL^{-} Naïve B cells were cross-referenced with germinal center B-cell-specific genes from the HPA. All expressed genes demonstrated tissue specificity. Reliability classifications are indicated by evidence codes: dark orange (enhanced validation), orange (supported), light orange (approved), and gray (uncertain). Genes not detected in the analysis were excluded. (Top 25 upregulated genes: *SELL, CCR7, ADAM28, PDE4B, PALM2-AKAP2, PLPP5, COBLL1, SEL1L3, PIK3IP1, BCL2, STK17A, TENT5C, IL6, CTSH, TP53INP1, ADK, IL13RA1, COL19A1, FCRL3, KLF3, ZBTB16, MGAT5, NT5E, CENPM, TXNDC5*). **** $P < 0.0001$. ATP, adenosine triphosphate; LogFC, Log2 fold change; NES, Normalized Enrichment Score; GSEA, Gene Set Enrichment Analysis; HPA, Human Protein Atlas.

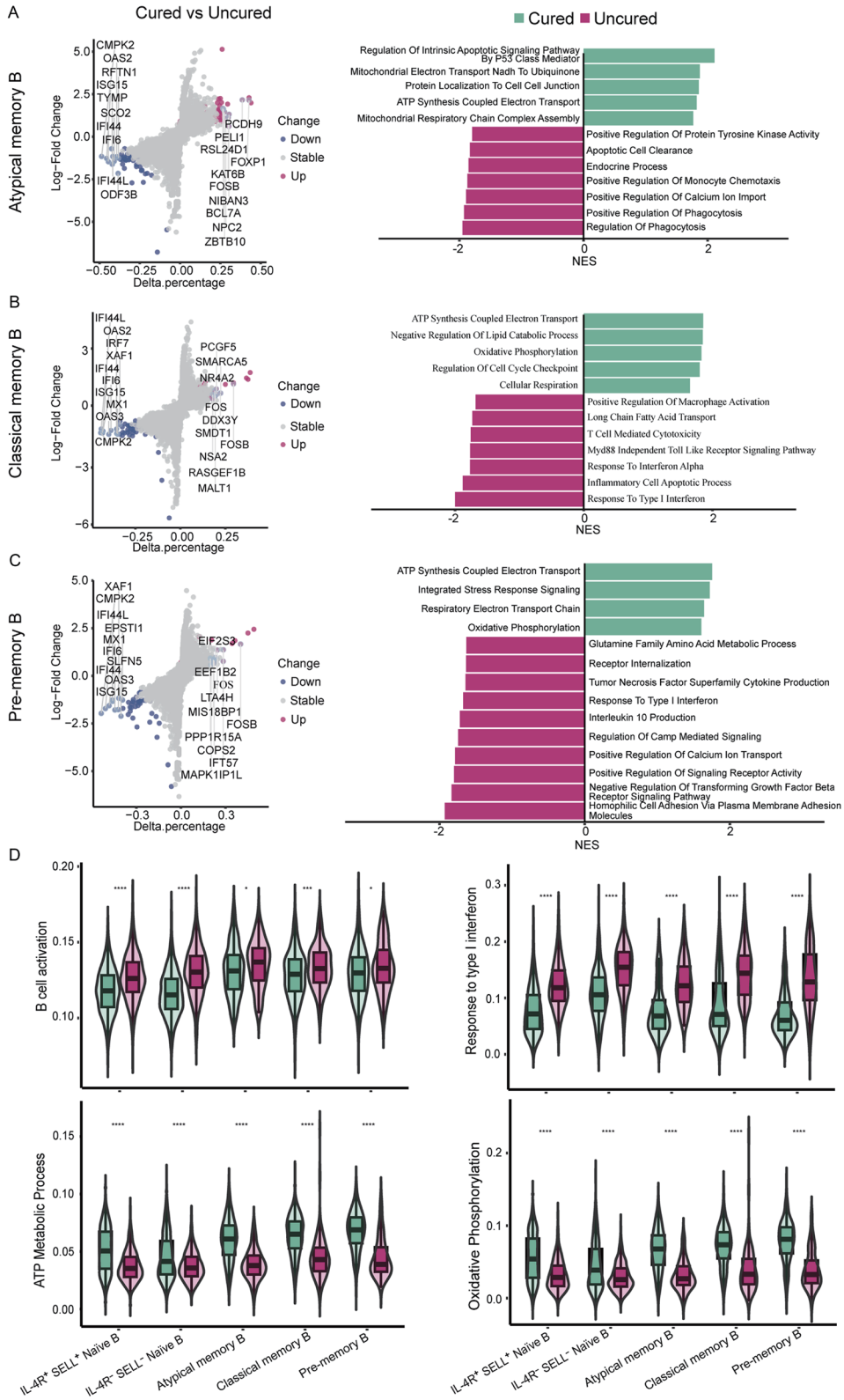

Fig. 3. Functional profiles of memory B cells in cured versus uncured patients. (A–C) Volcano plots from DESeq2 analysis comparing gene expression profiles of the three memory B-cell subsets between cured and uncured patients (left). Representative GSEA results for the three memory B-cell clusters are shown on the right. (D) Pathway activity scores of Naïve B cells and the three memory B-cell subsets in cured versus uncured groups. Scores were calculated using AUCell, and differences between groups were assessed using the Mann–Whitney U test. * $P < 0.05$; *** $P < 0.001$; **** $P < 0.0001$. ATP, adenosine triphosphate; NES, Normalized Enrichment Score.

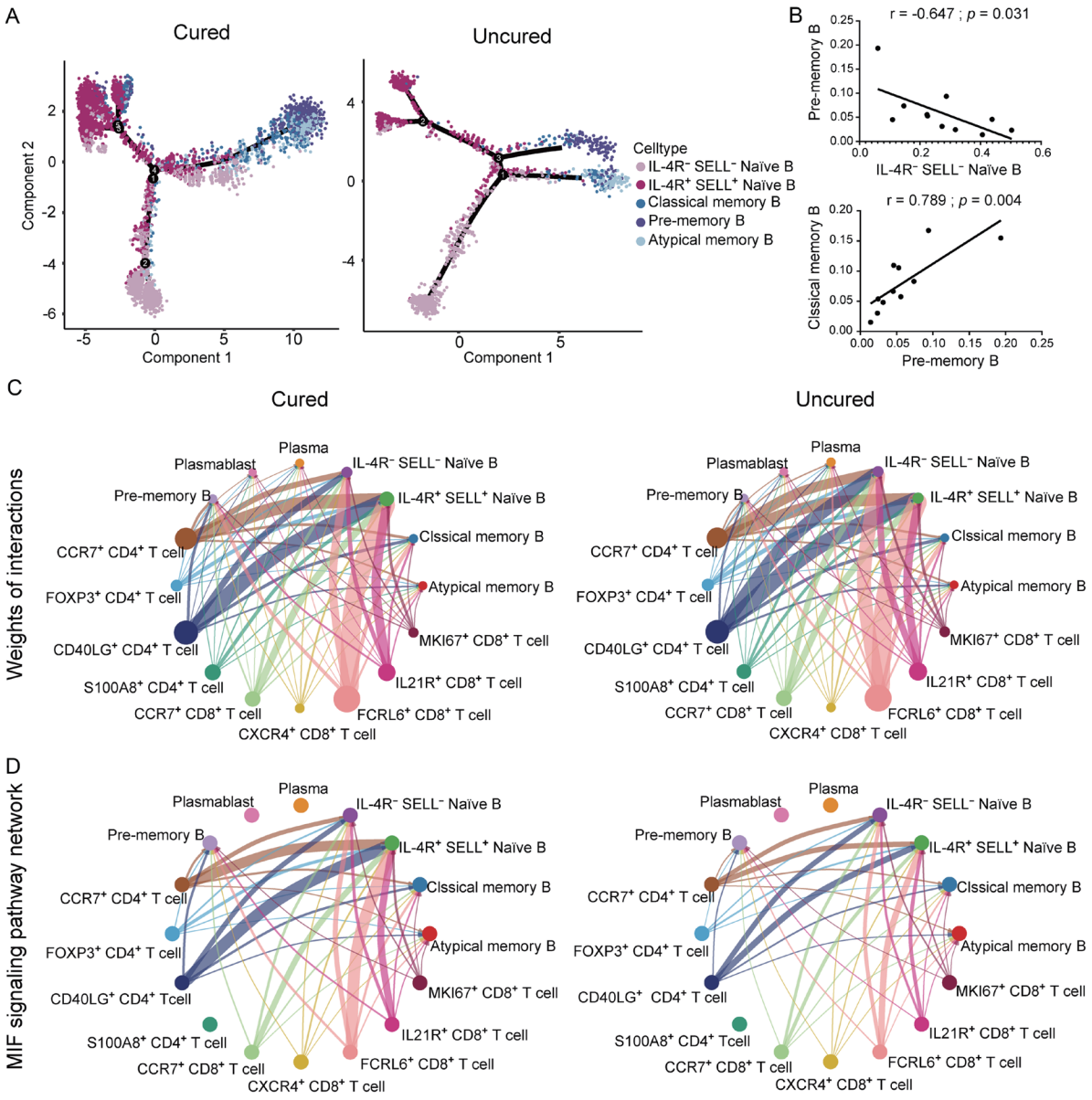

Fig. 4. Divergent trajectories of IL-4R^{+}SELL^{+} Naïve B cells and T-cell help in cured versus uncured patients. (A) Monocle pseudotime trajectory analysis of Naïve B-cell and memory B-cell differentiation. The state with the highest IGHD^{+} B-cell proportion was designated as the start. (B) Correlation analysis of B-cell subsets. (C) Cell–cell communication network between T- and B-cell subsets analyzed with CellChat, showing interaction weights (B cells as targets; CD4^{+}/CD8^{+} T cells as sources). (D) MIF signaling pathway-mediated B–T-cell interaction weights. Correlations between two quantitative variables were evaluated using Spearman's rank correlation test. Statistical significance was set at $P < 0.05$. MIF, Macrophage Migration Inhibitory Factor.

ble 3, and the flow cytometry gating strategy is shown in Figure 5A. No significant differences were observed in the frequencies of Naïve B cells (CD19^{+}CD21^{+}CD27^{-}), classical memory B cells (CD19^{+}CD21^{+}CD27^{+}), resting memory B cells (CD19^{+}CD21^{-}CD27^{+}), or atypical memory B cells (CD19^{+}CD21^{-}CD27^{-}) between cured and uncured groups (Supplementary Fig. 4A). Furthermore, no significant correlation was observed between HBsAg levels at sampling and the frequencies of these four B-cell subsets (Supplementary Fig. 4B). We further stratified Naïve B cells based on IL-4R and SELL expression. Comparative analysis between functionally cured and uncured groups revealed significantly higher frequencies of IL-4R^{+}SELL^{+} Naïve B cells in cured patients (P = 0.003) (Fig. 5B). Correlation analyses demonstrated inverse relationships between IL-4R^{+}SELL^{+} Naïve B-cell frequency and baseline HBsAg levels (r = −0.546, P = 0.002) (Fig. 5C), as well as HBsAg levels at sampling (r = −0.562, P = 0.023) (Fig. 5D). Uncured patients exhibited a higher percentage of IL-4R^{-}SELL^{-} Naïve B cells compared with cured patients (P = 0.008) (Fig. 5E). This subset showed positive correlations with baseline HBsAg levels (r = 0.651, P = 0.0002) (Fig. 5F) and sampling time point (r = 0.565, P = 0.022) (Fig. 5G). In the cured group, paired specimens were collected from 7 patients at two time points: an early time point before HBsAg loss (Cured_T1) and the time of HBsAg loss (Cured). Similarly,

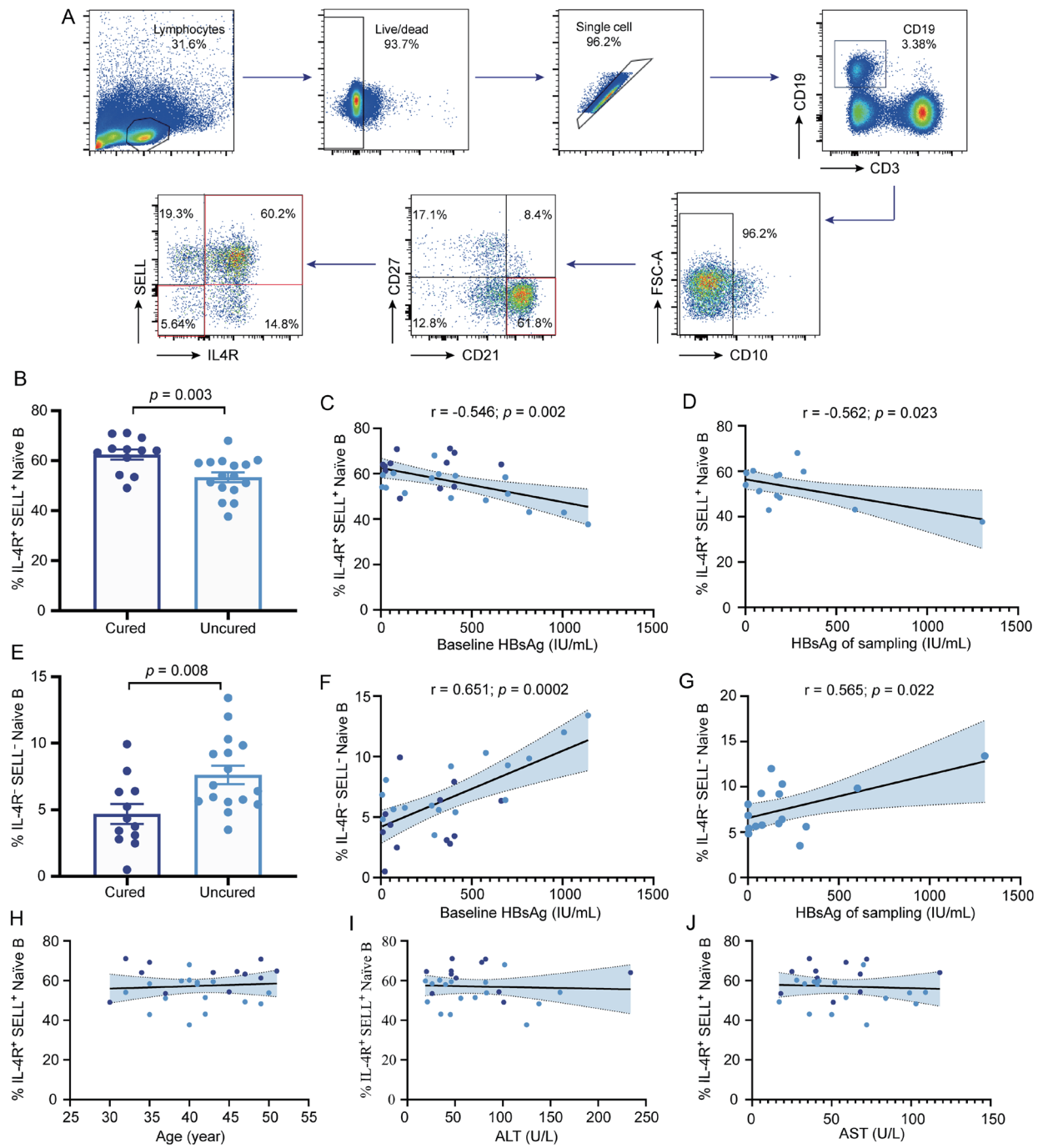

Fig. 5. High frequency of IL-4R$^+$SELL$^+$ Naïve B cells was further confirmed in cured patients with CHB. (A) Gating strategy for flow cytometry. (B) Comparative frequencies of IL-4R$^+$SELL$^+$ Naïve B cells across clinical response groups (cured and uncured). (C–D) Spearman correlation between IL-4R$^+$SELL$^+$ Naïve B-cell frequencies and levels of baseline HBsAg and sampling point. (E) Comparative frequencies of IL-4R$^-$SELL$^-$ Naïve B cells among cured and uncured groups. (F–G) Spearman correlation between IL-4R$^-$SELL$^-$ Naïve B-cell frequencies and levels of baseline HBsAg and sampling point. Spearman correlation between IL-4R$^+$SELL$^+$ Naïve B-cell frequency and patient age (H), ALT levels at the sampling time point (I), and AST levels at the sampling time point (J). Baseline HBsAg refers to the HBsAg level at the initiation of PEG-IFNα therapy. Data are presented as mean ± SEM, and differences were analyzed with the Mann–Whitney U test. Correlations between two quantitative variables were evaluated using Spearman's rank correlation test. Statistical significance was set at $P < 0.05$. HBsAg, Hepatitis B surface antigen; ALT, Alanine aminotransferase; AST, Aspartate aminotransferase; CHB, chronic hepatitis B; PEG-IFNα, Pegylated interferon-alpha.

paired specimens were collected from uncured patients at corresponding time points (Uncured_T1 and Uncured). We then compared changes in IL-4R$^+$SELL$^+$ Naïve B-cell frequencies between the two time points in each group. In both groups, the frequencies of these cells remained relatively stable over time (Supplementary Fig. 4C and D). Finally, the frequencies of IL-4R$^+$SELL$^+$ Naïve B cells showed no correlation with age, ALT, or AST (Fig. 5H–J).

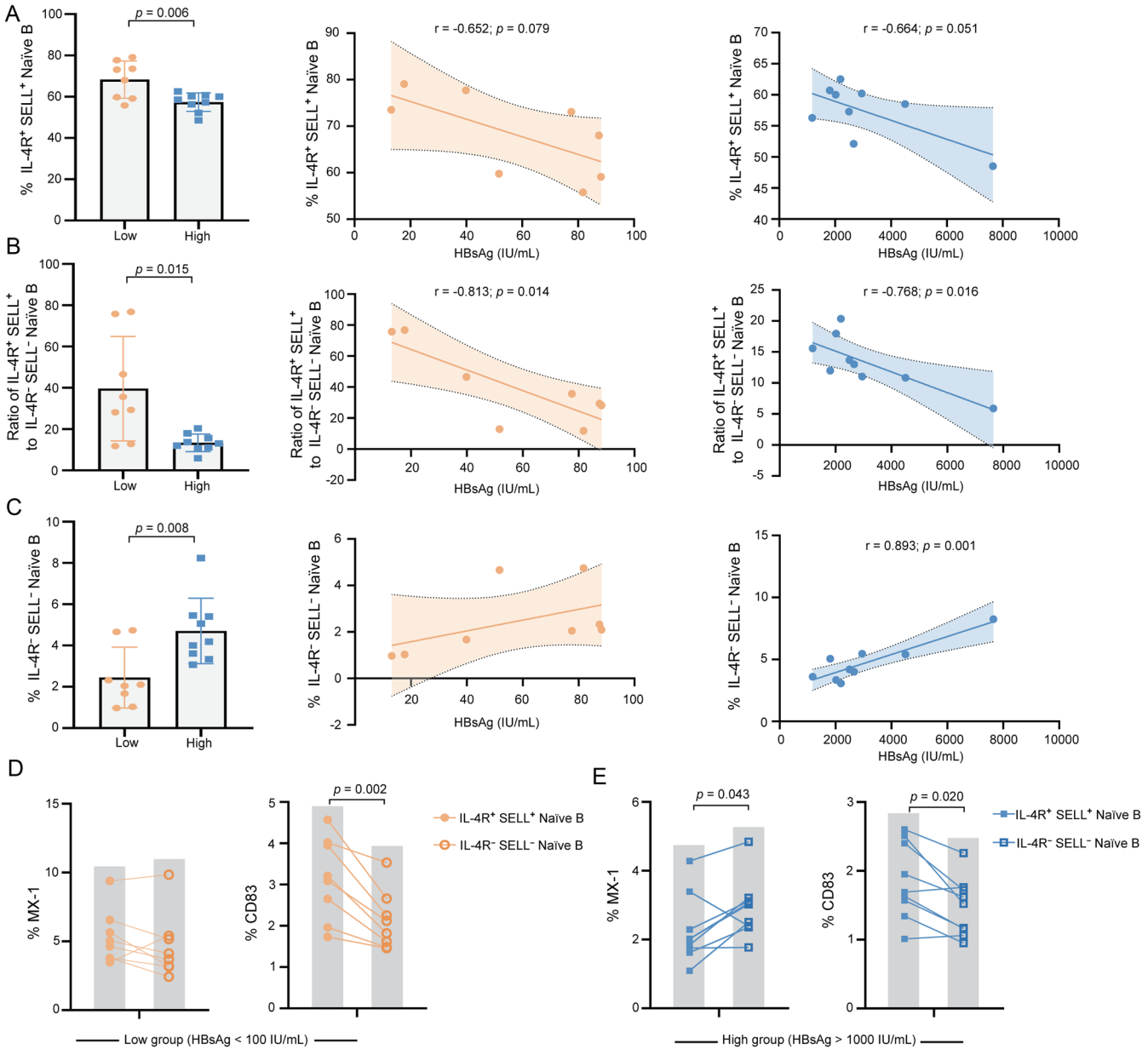

Fig. 6. IL-4R^{+}SELL^{+} Naïve B cells are associated with low HBsAg levels in patients with CHB. (A) Frequency comparison of IL-4R^{+}SELL^{+} Naïve B cells between low- and high-HBsAg groups (left), correlation with quantitative HBsAg levels in the low-HBsAg cohort (middle), and correlation with quantitative HBsAg levels in the high-HBsAg cohort (right). (B) Ratio of IL-4R^{+}SELL^{+} Naïve B cells to IL-4R^{-}SELL^{-} Naïve B cells between the two groups (left) and correlation of this ratio with HBsAg levels in the low-HBsAg (middle) and high-HBsAg (right) groups. (C) Comparative analysis of IL-4R^{-}SELL^{-} Naïve B-cell frequencies between low- and high-HBsAg groups (left). Correlation of these frequencies with HBsAg levels in the low-HBsAg group (middle) and high-HBsAg group (right). Comparative analysis of MX-1 and CD83 expression between IL-4R^{+}SELL^{+} Naïve B cells and IL-4R^{-}SELL^{-} Naïve B cells in the low-HBsAg group (D) and high-HBsAg group (E). Low: <100 IU/mL; high: >1,000 IU/mL. Data are presented as mean ± SEM, and differences were analyzed with the Mann–Whitney U test. Correlations between two quantitative variables were evaluated using Spearman's rank correlation test. Statistical significance was set at $P < 0.05$. CHB, chronic hepatitis B; HBsAg, Hepatitis B surface antigen; SEM, standard error of the mean.

IL-4R^{+}SELL^{+} Naïve B cells are associated with low levels of HBsAg in patients with CHB

In NAs-experienced CHB patients, a baseline HBsAg level ≤ 100 IU/mL is associated with a higher likelihood of achieving functional cure.[22–25] To further validate the relationship between IL-4R^{+}SELL^{+} Naïve B cells and antigen burden in treated patients, we analyzed an additional independent cohort stratified by HBsAg levels (Supplementary Table 1). The cohort was divided into a low HBsAg group (<100 IU/mL; median, 64.6 IU/mL; IQR, 23.3–86.0) and a high HBsAg group (>1,000 IU/mL; median, 2,497.0 IU/mL; IQR, 1,915.0–3,725.0).

The gating strategy for B-cell subsets is shown in Supplementary Figure 5. At the overall B-cell subset level, no significant differences were observed in the frequencies of Naïve, classical memory, resting memory, or atypical memory B cells between the low and high HBsAg groups (Supplementary Fig. 6A), and no correlations were observed between

the frequencies of these subsets and HBsAg levels (Supplementary Fig. 6B and C). In contrast, clear differences were observed within the Naïve B-cell compartment. Patients with low HBsAg levels exhibited significantly higher percentages of IL-4R$^+$SELL$^+$ Naïve B cells (P = 0.006) and an elevated IL-4R$^+$SELL$^+$/IL-4R$^-$SELL$^-$ Naïve B-cell ratio (P = 0.015). Consistently, both the frequency of IL-4R$^+$SELL$^+$ Naïve B cells and the IL-4R$^+$SELL$^+$/IL-4R$^-$SELL$^-$ ratio showed inverse correlations with HBsAg levels at sampling. However, only the latter reached statistical significance (r = −0.813, P = 0.014), whereas the former did not (r = −0.652, P = 0.079) (Fig. 6A and B). Conversely, the frequency of IL-4R$^-$SELL$^-$ Naïve B cells was increased in patients with high HBsAg levels and showed a positive correlation with HBsAg levels (r = 0.893, P = 0.001) (Fig. 6C).

To explore phenotypic differences within Naïve B-cell subsets under different antigen burdens, we examined activation- and interferon-related markers. IL-4R$^+$SELL$^+$ Naïve B cells consistently expressed higher levels of CD83 than IL-4R$^-$SELL$^-$ Naïve B cells in both low- and high-HBsAg patients (P = 0.002 and P = 0.02). Conversely, within the high-HBsAg group, IL-4R$^-$SELL$^-$ Naïve B cells showed higher expression of MX1 than IL-4R$^+$SELL$^+$ Naïve B cells (P = 0.043), suggesting stronger interferon-associated activation in this subset under elevated antigen load (Fig. 6D and E).

Discussion

By integrating single-cell transcriptomics and flow cytometry, we identified two transcriptionally and phenotypically distinct Naïve B-cell subsets characterized by IL-4R and SELL expression. The IL-4R$^+$SELL$^+$ subset displayed transcriptional and phenotypic features indicative of enhanced activation potential and germinal-center-related differentiation programs, highlighting its potential role in shaping effective antiviral humoral immunity. Comparative transcriptional analyses revealed that Naïve B cells from functionally cured patients showed enrichment of bioenergetic pathways, including oxidative phosphorylation and ATP synthesis, whereas persistent activation of interferon signaling was observed in uncured individuals.

B cells are essential for functional cure in CHB, largely through maintaining HBV-specific humoral immunity.[15] Although previous studies have focused on memory B-cell dysfunction, accumulating evidence suggests that Naïve B cells also actively contribute to antiviral responses. Recent work indicates that pre-existing circulating antibodies can mask immunodominant epitopes, limiting the participation of Naïve B cells targeting these sites. When antigen levels decline, Naïve B cells may be redirected toward previously subdominant epitopes and restore their functional activity.[26,27] In line with this, changes in Naïve B-cell activation states have been associated with immune improvement in CHB patients.[18] In our study, IL-4R$^+$SELL$^+$ Naïve B cells were present at higher levels in functionally cured patients and showed an inverse correlation with HBsAg levels at the sampling time point, suggesting that Naïve B-cell remodeling is closely associated with treatment responses to PEG-IFNα therapy, although the directionality of this association remains to be clarified.

Beyond transcriptional programs, emerging evidence highlights the importance of cellular metabolism in shaping B-cell fate. Cellular metabolic fitness has been increasingly recognized as an important determinant of germinal center B-cell selection and antibody affinity maturation. Previous studies have shown that enhanced oxidative phosphorylation supports positive selection within germinal centers and promotes processes such as class-switch recombination.[28,29] Consistent with these observations, our results show that oxidative phosphorylation pathways are upregulated in Naïve B cells from cured patients, suggesting a cellular state favorable for efficient germinal center differentiation and humoral immune responses.

In addition, IL-4R$^+$SELL$^+$ Naïve B cells displayed increased expression of chemokine receptors and activation markers associated with germinal center homing, including *CCR7, CXCR5*, and *CD69*.[30] Correspondingly, CD40LG$^+$CD4$^+$ T cells in cured patients showed transcriptional features consistent with enhanced helper activity. These findings raise the possibility that IL-4R$^+$SELL$^+$ Naïve B cells may serve as a precursor population capable of efficiently entering germinal center reactions under appropriate T-cell help. Notably, intact IL-4 signaling has been shown to support Naïve B-cell survival and differentiation, whereas IL-4R blockade reduces IL-4R-expressing Naïve B cells and impairs long-term antibody responses.[21,31,32] In our previous study of CHB patients receiving PEG-IFNα add-on therapy, serum IL-4 showed a transient rise from baseline to week 12, with a more pronounced peak in patients who later achieved HBsAg loss. This early IL-4 increase suggests that the cytokine environment during PEG-IFNα treatment may favor IL-4-responsive B-cell populations.[33] Although our data do not directly demonstrate IL-4 dependence, these observations are consistent with the possibility that preserved IL-4 responsiveness contributes to the enhanced competence of the IL-4R$^+$SELL$^+$ Naïve B-cell subset. Clinically, we observed that the frequency of IL-4R$^+$SELL$^+$ Naïve B cells was significantly increased in patients who ultimately achieved functional cure, and this high frequency was stable in samples collected during treatment prior to HBsAg loss. As the switch from Naïve B cells to antibody-secreting plasma cells requires multiple rounds of selection and differentiation, the potential contribution of IL-4R$^+$SELL$^+$ Naïve B cells to antibody production requires further investigation. In this context, we also observed an inverse association between IL-4R$^+$SELL$^+$ Naïve B-cell frequency and circulating HBsAg levels. Consistent with this observation, higher levels of this subset were also observed in patients with low HBsAg levels. Importantly, this association did not correlate with cumulative PEG-IFNα treatment duration at sampling. Together, these findings suggest that this observation is unlikely to be solely driven by cumulative interferon exposure but may reflect either a treatment-associated state or a pre-existing immune population. Overall, a high frequency of IL-4R$^+$SELL$^+$ Naïve B cells in combination with low HBsAg levels may indicate a favorable immune state associated with functional cure.

Several limitations should be acknowledged. First, the present dataset was derived from a retrospective cohort and lacked longitudinal sampling at treatment initiation and during the early response phase. Therefore, it remains unclear whether the increased frequency of IL-4R$^+$SELL$^+$ Naïve B cells in cured patients represents a pre-existing immune state associated with functional cure or a treatment-associated immune change. Although temporal associations were observed in a limited number of paired samples, these findings should be validated in independent longitudinal cohorts. Second, the relatively small sample size and lack of mechanistic experiments limit the interpretation of causality. Larger prospective cohorts and functional studies will be required to confirm the clinical significance of this B-cell subset.

Conclusions

Our study reveals previously unappreciated heterogeneity within the Naïve B-cell compartment in CHB. We identify

a distinct IL-4R$^+$SELL$^+$ Naïve B-cell subset associated with lower HBsAg levels, enhanced T-cell help, and transcriptional features indicative of germinal center competence. These findings expand the current understanding of B-cell biology in CHB and highlight Naïve B cells as a potentially important component of antiviral immune remodeling associated with functional cure.

Supporting information

Supplementary material for this article is available at https://doi.org/10.14218/JCTH.2026.00356.

Acknowledgments

We thank all patients who participated in this study. We would also like to thank Dr. Liguo Zhang from the Institute of Biophysics, Chinese Academy of Sciences, for providing the recombinant human MX-1 protein. Preprint: https://doi.org/10.21203/rs.3.rs-7813973/v1.

Funding

This work was supported by grants from the National Science and Technology Major Project of China (no. 2025ZD01905602) and the National Natural Science Foundation of China (nos. 82572549 and 82502143).

Conflict of interest

FSW has been an Editor-in-Chief of *Journal of Clinical and Translational Hepatology* since 2026. The other authors have no conflict of interests related to this publication.

Author contributions

Study concept and design (RX, FSW), acquisition of data (HL, HW, YY, JY, YG, YC, LC), analysis and interpretation of data (LT, CB), drafting of the manuscript (RX, LT), critical revision of the manuscript for important intellectual content (CZhang, YZ, JS, YJ, TY, JL, JLF), technical support (CZhen), and study supervision (FSW). All authors made significant contributions to this study and approved the final manuscript.

Ethical statement

This retrospective study was approved by the Ethics Committee of the Fifth Medical Center of PLA General Hospital (Approval No. KY-2023-12-86-6), which waived the requirement for patient consent. The study complied with the Declaration of Helsinki (as revised in 2024) and relevant laws, with strict protection of patient information confidentiality.

Data sharing statement

The scRNA-seq datasets generated or analyzed during the current study are available from the corresponding author upon reasonable request.

References

[1] Polaris Observatory Collaborators. Global prevalence, treatment, and prevention of hepatitis B virus infection in 2016: a modelling study. Lancet Gastroenterol Hepatol 2018;3(6):383–403. doi:10.1016/S2468-1253(18)30056-6, PMID:29599078.
[2] Huang D, Wu D, Wang P, Wang Y, Yuan W, Hu D, *et al*. End-of-treatment HBcrAg and HBsAb levels identify durable functional cure after Peg-IFN-based therapy in patients with CHB. J Hepatol 2022;77(1):42–54. doi:10.1016/j.jhep.2022.01.021, PMID:35149125.
[3] Chinese Society of Hepatology, Chinese Medical Association, Chinese Society of Infectious Diseases, Chinese Medical Association. [Guidelines for the prevention and treatment of chronic hepatitis B (version 2022)]. Chin J Hepatol 2022;30(12):1309–1331. doi:10.3760/cma.j.cn501113-20221204-00607, PMID:36891718.
[4] Huang H, Li X, Zhu J, Ye S, Zhang H, Wang W, *et al*. Entecavir vs lamivudine for prevention of hepatitis B virus reactivation among patients with untreated diffuse large B-cell lymphoma receiving R-CHOP chemotherapy: a randomized clinical trial. JAMA 2014;312(23):2521–2530. doi:10.1001/jama.2014.15704, PMID:25514302.
[5] Loomba R, Liang TJ. Hepatitis B Reactivation Associated With Immune Suppressive and Biological Modifier Therapies: Current Concepts, Management Strategies, and Future Directions. Gastroenterology 2017;152(6):1297–1309. doi:10.1053/j.gastro.2017.02.009, PMID:28219691.
[6] Kusumoto S, Arcaini L, Hong X, Jin J, Kim WS, Kwong YL, *et al*. Risk of HBV reactivation in patients with B-cell lymphomas receiving obinutuzumab or rituximab immunochemotherapy. Blood 2019;133(2):137–146. doi:10.1182/blood-2018-04-848044, PMID:30341058.
[7] Dervite I, Hober D, Morel P. Acute hepatitis B in a patient with antibodies to hepatitis B surface antigen who was receiving rituximab. N Engl J Med 2001;344(1):68–69. doi:10.1056/NEJM200101043440120, PMID:11187122.
[8] Oliviero B, Cerino A, Varchetta S, Paudice E, Pai S, Ludovisi S, *et al*. Enhanced B-cell differentiation and reduced proliferative capacity in chronic hepatitis C and chronic hepatitis B virus infections. J Hepatol 2011;55(1):53–60. doi:10.1016/j.jhep.2010.10.016, PMID:21145853.
[9] Xu X, Shang Q, Chen X, Nie W, Zou Z, Huang A, *et al*. Reversal of B-cell hyperactivation and functional impairment is associated with HBsAg seroconversion in chronic hepatitis B patients. Cell Mol Immunol 2015;12(3):309–316. doi:10.1038/cmi.2015.25, PMID:25849120.
[10] Vanwolleghem T, Hou J, van Oord G, Andeweg AC, Osterhaus AD, Pas SD, *et al*. Re-evaluation of hepatitis B virus clinical phases by systems biology identifies unappreciated roles for the innate immune response and B cells. Hepatology 2015;62(1):87–100. doi:10.1002/hep.27805, PMID:25808668.
[11] Salimzadeh L, Le Bert N, Dutertre CA, Gill US, Newell EW, Frey C, *et al*. PD-1 blockade partially recovers dysfunctional virus-specific B cells in chronic hepatitis B infection. J Clin Invest 2018;128(10):4573–4587. doi:10.1172/JCI121957, PMID:30084841.
[12] Burton AR, Pallett LJ, McCoy LE, Suveizdyte K, Amin OE, Swadling L, *et al*. Circulating and intrahepatic antiviral B cells are defective in hepatitis B. J Clin Invest 2018;128(10):4588–4603. doi:10.1172/jci121960, PMID:30091725.
[13] Vanwolleghem T, Groothuismink ZMA, Kreefft K, Hung M, Novikov N, Boonstra A. Hepatitis B core-specific memory B cell responses associate with clinical parameters in patients with chronic HBV. J Hepatol 2020;73(1):52–61. doi:10.1016/j.jhep.2020.01.024, PMID:32061650.
[14] Dusheiko GM, Hoofnagle JH, Cooksley WG, James SP, Jones EA. Synthesis of antibodies to hepatitis B virus by cultured lymphocytes from chronic hepatitis B surface antigen carriers. J Clin Invest 1983;71(5):1104–1113. doi:10.1172/jci110860, PMID:6602149.
[15] Vanwolleghem T, Adomati T, Van Hees S, Janssen HLA. Humoral immunity in hepatitis B virus infection: Rehabilitating the B in HBV. JHEP Rep 2022;4(2):100398. doi:10.1016/j.jhepr.2021.100398, PMID:35059620.
[16] Le Bert N, Salimzadeh L, Gill US, Dutertre CA, Facchetti F, Tan A, *et al*. Comparative characterization of B cells specific for HBV nucleocapsid and envelope proteins in patients with chronic hepatitis B. J Hepatol 2020;72(1):34–44. doi:10.1016/j.jhep.2019.07.015, PMID:31348999.
[17] Zhang JW, Lai RM, Wang LF, Wang SL, Xue HX, Li C, *et al*. Varied immune responses of HBV-specific B cells in patients undergoing pegylated interferon-alpha treatment for chronic hepatitis B. J Hepatol 2024;81(6):960–970. doi:10.1016/j.jhep.2024.06.033, PMID:38992769.
[18] Spangler A, Shimberg GD, Mantus GE, Malek R, Cominsky LY, Tsybovsky Y, *et al*. Early influenza virus exposure shapes the B cell response to influenza vaccination in individuals 50 years later. Immunity 2025;58(3):728–744.e9. doi:10.1016/j.immuni.2025.02.004, PMID:40023164.
[19] Basu M, Fucile C, Piepenbrink MS, Bunce CA, Man LX, Liesveld J, *et al*. Mixed Origins: HIV gp120-Specific Memory Develops from Pre-Existing Memory and Naive B Cells Following Vaccination in Humans. AIDS Res Hum Retroviruses 2023;39(7):350–366. doi:10.1089/AID.2022.0104, PMID:36762930.
[20] Morgan D, Tergaonkar V. Unraveling B cell trajectories at single cell resolution. Trends Immunol 2022;43(3):210–229. doi:10.1016/j.it.2022.01.003, PMID:35090788.
[21] Mountz JD, Gao M, Ponder DM, Liu S, Sun CW, Alduraibi F, *et al*. IL-4 receptor blockade is a global repressor of naïve B cell development and responses in a dupilumab-treated patient. Clin Immunol 2022;244:109130. doi:10.1016/j.clim.2022.109130, PMID:36189576.
[22] Han L, Wang Z, Kang L, Cui X, Li Y, Yin H, *et al*. Predicting relapse after achieving a functional cure for chronic hepatitis B (CHB) using baseline HBsAg and end-of-treatment HBsAb levels. Sci Rep 2025;15(1):13873. doi:10.1038/s41598-025-86555-1, PMID:40263318.
[23] Tang Q, Ye J, Zhang Y, Zhang P, Xia G, Zhu J, *et al*. Establishment of a multi-parameter prediction model for the functional cure of HBeAg-negative chronic hepatitis B patients treated with pegylated interferona and decision process based on response-guided therapy strategy. BMC Infect Dis 2023;23(1):456. doi:10.1186/s12879-023-08443-1, PMID:37430256.
[24] Zhang PX, Tang QQ, Zhu J, Deng WY, Zhang ZH. Predictive models for functional cure in patients with CHB receiving PEG-IFN therapy based on HBsAg quantification through meta-analysis. Hepatol Int 2024;18(4):1110–1121. doi:10.1007/s12072-024-10666-6, PMID:38913149.

[25] Wen C, Wang Y, Tian H, Lei Y, Wang Z, Cai D, *et al*. Clinical cure induced by pegylated interferon α-2b in the advantaged population of chronic hepatitis B virus infection: a retrospective cohort study. Front Cell Infect Microbiol 2023;13:1332232. doi:10.3389/fcimb.2023.1332232, PMID:38292859.
[26] Turner JS, Zhou JQ, Han J, Schmitz AJ, Rizk AA, Alsoussi WB, *et al*. Human germinal centres engage memory and naive B cells after influenza vaccination. Nature 2020;586(7827):127–132. doi:10.1038/s41586-020-2711-0, PMID:32866963.
[27] Tas JMJ, Koo JH, Lin YC, Xie Z, Steichen JM, Jackson AM, *et al*. Antibodies from primary humoral responses modulate the recruitment of naive B cells during secondary responses. Immunity 2022;55(10):1856–1871.e6. doi:10.1016/j.immuni.2022.07.020, PMID:35987201.
[28] Gracie CJ, Mitchell R, Johnstone JC, Clarke AJ. The unusual metabolism of germinal center B cells. Trends Immunol 2025;46(5):416–428. doi:10.1016/j.it.2025.02.015, PMID:40221291.
[29] Zhang C, Zhang TX, Liu Y, Jia D, Zeng P, Du C, *et al*. B-Cell Compartmental Features and Molecular Basis for Therapy in Autoimmune Disease. Neurol Neuroimmunol Neuroinflamm 2021;8(6):e1070. doi:10.1212/NXI.0000000000001070, PMID:34465614.
[30] O'Connor MH, Muir R, Chakhtoura M, Fang M, Moysi E, Moir S, *et al*. A follicular regulatory Innate Lymphoid Cell population impairs interactions between germinal center Tfh and B cells. Commun Biol 2021;4(1):563. doi:10.1038/s42003-021-02079-0, PMID:33980982.
[31] Guo B, Rothstein TL. IL-4 upregulates Igα and Igβ protein, resulting in augmented IgM maturation and B cell receptor-triggered B cell activation. J Immunol 2013;191(2):670–677. doi:10.4049/jimmunol.1203211, PMID:23776171.
[32] Liechti T, Kadelka C, Braun DL, Kuster H, Böni J, Robbiani M, *et al*. Widespread B cell perturbations in HIV-1 infection afflict naive and marginal zone B cells. J Exp Med 2019;216(9):2071–2090. doi:10.1084/jem.20181124, PMID:31221742.
[33] Wang WX, Jia R, Jin XY, Li X, Zhou SN, Zhang XN, *et al*. Serum cytokine change profile associated with HBsAg loss during combination therapy with PEG-IFN-α in NAs-suppressed chronic hepatitis B patients. Front Immunol 2023;14:1121778. doi:10.3389/fimmu.2023.1121778, PMID:36756119.